HFSW Radar model and evaluation of a new detection approach based on source analysis and extraction

S. Grosdidier, A. Baussard, A. Khenchaf
E^3I^2 Laboratory – ENSIETA
2 rue François Verny, 29806 Brest Cedex- France
E-mail: grosdisa@ensieta.fr

***Abstract*— High Frequency radar, which is based on surface wave propagation, is an important tool for remote sensing sea state. It can also be used to detect targets far beyond the conventional microwave radar coverage. The goal of our project is to investigate this detection capability. In this way, the received power by this kind of system in presence of targets has been modeled leading to a Range-Doppler image. This model can be used for different purpose like for example the (theoretical) evaluation of target detection algorithms. In this contribution, the developed model is presented, and the detection part is discussed.**

Keywords-HF radar; ground-wave propagation; HF modeling; target detection; curvelet and wavelet processing.

I. INTRODUCTION

High Frequency Surface Wave (HFSW) radars have been efficiently used these last three decades for remote sensing the sea state. They are usually set up along the coast and can provide oceanographic parameters like surface currents, wave spectra, wind intensity and direction …

Recently, these systems proved to be potentially useful in target detection and tracking [8, 9, 14, 15]. The main interest is that they provide a long-range compared to microwave radars. Actually, they can cover areas up to 200 nautical miles in range. This range value corresponds to the Exclusive Economic Zone (EEZ). Continuous maritime surveillance of activities within the EEZ is a key question for civil or military applications. HFSW radars can provide a cheaper and more practical way to monitor such area than usual multi-sensor system (composed for example by several patrol crafts and ships, and microwave radar).

Numbers of HF systems have been already developed essentially for oceanographic applications. In this contribution, the so-called WERA system [11] is considered. The goal in our project is to evaluate this system for target detection and tracking without altering the radar parameters (fixed for oceanographic parameters estimation). This mean that our system is not optimized for target detection (one can particularly notice a low emitted power). This is a challenging problem since the signal environment includes a significant background noise, different kinds of clutter and interference, which will strongly limit the detection capabilities.

As for oceanographic task we will work on Range-Doppler images. This image gives the spectral density of the power backscattered by scatterers, situated on an area schematized in fig 1 (red surrounded area) according to range and the Doppler frequency. In this area the scatterers are essentially ocean waves and targets. In this contribution, a Range-Doppler image is simulated. This HFSW radars model can be used in different ways like, for example, to evaluate the performances of target detection algorithms (since with real data is not possible to know for sure all the targets in the area of interest). The model takes into account the three major contributions: the background noise, the sea clutter, the target. Moreover some experimental processing effects have been added.

Starting from this model and experimental data, the detection problem is discussed in the last section of this paper. Finally some concluding remarks complete the paper.

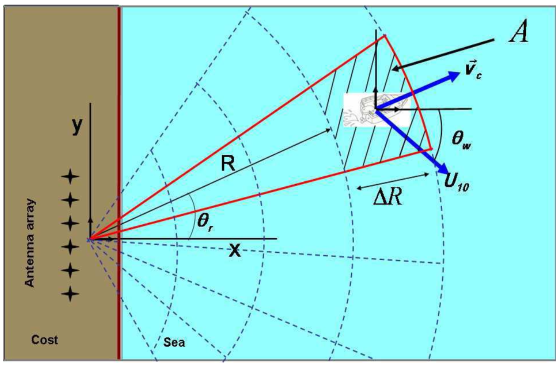

Figure 1. HF radar setup.

II. SPECTRAL DENSITY FROM THE SEA CLUTTER

This section gives a short overview on theoretical issues used in the model.

A. *Radar equation*

For monostatic HFSW radars, the spectral density of the power backscattered by a sea surface can be written as

$$P_r(\omega_d, R) = \frac{\lambda_r^{\ 2} P_t G_t G_r |F(R)|^4}{(4\pi)^3 R^4} \sigma_s(\omega_d) A, \qquad (1)$$

where λ_r is the radar wavelength, R is the range, P_t is the transmitted power and G_t and G_r are respectively the transmitter and receiver antenna gain. $\sigma_s(\omega_d)$ stands for the radar cross-section of the radar patch (in $m^{-3}Hz^{-1}$) according to the Doppler pulsation ω_d. A is the area of the patch (see fig 1) and $F(R)$ is the surface wave attenuation function.

B. *Attenuation function*

The attenuation function must take into account different phenomena which attenuate the electromagnetic wave when it propagates along the sea surface. Sommerfeld [1] gives the vertical electric field E_z over a flat, smooth surface with finite conductivity and far from the source. It can be written as

$$E_z(R) = F_1(R, \Delta) E_0(R), \qquad (2)$$

where E_0 is the vertical electric field over a flat perfectly conducting surface and F_1 is the so-called Sommerfeld function which depends on the normalized surface impedance [2] :

$$\Delta = \frac{1}{n}\sqrt{1 - \frac{1}{n^2}}, \qquad (3)$$

where n is the refractive complex index of the sea.

To take into account the roughness of the sea surface the effective impedance $\overline{\Delta}$ proposed by Barrick in [3] can be used instead of Δ. The effective impedance was calculated by Barrick thanks to the boundary perturbation technique of Rice. Shortly it can be written as

$$\overline{\Delta} = \Delta + \int_{-\infty}^{+\infty}\int_{-\infty}^{+\infty} H(k, \theta - \theta_w) S(k, \theta - \theta_w) dk d\theta, \qquad (4)$$

where $H(k, \theta - \theta_w)$ is a function which depends on radar wave number k_r and Δ. The expression of the function H can be found in [3]. $S(k, \theta - \theta_w)$ is the sea spectrum (described in part C) and θ_w is the wind direction.

For long range the curvature of the earth must also be taken into account in the attenuation function. For this purpose the Bremmer series curvature correction was used. Finally, the attenuation function $F(R, \overline{\Delta})$ writes as [2]

$$F(R, \overline{\Delta}) = F_1 - \left(\frac{\delta^3}{2}\right)\left[1 - j(\pi p)^{1/2} - (1 + 2p)F_1\right] +$$
$$\delta^6\left[1 - j(\pi p)^{1/2}(1 - p) - 2p + \frac{5}{6}p^2 + \left(\frac{p^2}{2} - 1\right)F_1\right]$$

where p is the numerical distance of Sommerfeld, $\delta^3 = \left(j \big/ k_r a \overline{\Delta}^3 \right)$ and a is the earth radius.

In Fig. 2, the magnitude of the attenuation function as a function of radar distance is given to compare different effects of the phenomena described above. The sea conductivity is taken as 4 ohms and the relative permittivity is fixed to 70.

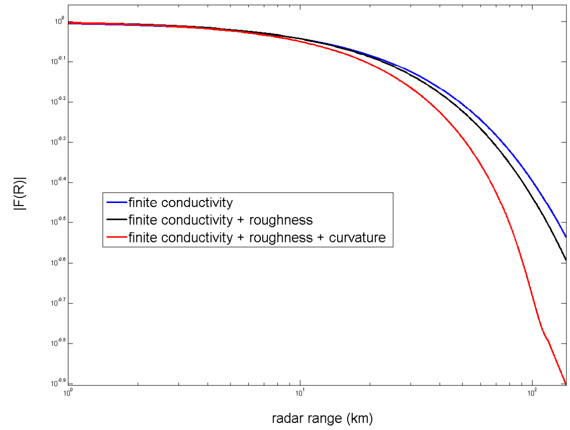

Figure 2. Attenuation function |F(R)| under the three different hypothesis. For the roughness, a 9m/s wind has been considered in a cross wind configuration.

C. *Radar cross section of the sea surface*

To model the radar cross section (RCS) of the sea, the theoretical results of Walsh *et al.* [4] have been considered. They are very similar with those of Barrick [5] for the monostatic case (which is considered in this contribution). The main difference is that Walsh *et al.* consider a pulsed source. The main hypotheses for the sea are small slope, small height and perfectly conducting.

The greatest physical effect in the radar cross section of the sea surface is produced by scattering from ocean waves having a wavelength which is half of the radar wavelength and moving radially to and away from the radar. These sea waves are called Bragg waves and their wave vector is given by

$$\vec{k}_b = 2\vec{k}_r,$$

where $\vec{k}_r$ is the wave vector of the radar.

This first-order resonant scattering effect results in two dominant peaks in the Doppler spectrum called the Bragg lines. Following [4], the first-order RCS is expressed as

$$\sigma_1(\omega_d) = 16\pi k_r \sum_{m=\pm 1} S(m\vec{k}) \frac{k^{5/2}}{\sqrt{g}} \Delta r \operatorname{sinc}^2\left(\frac{\Delta r}{2}(k - 2k_b)\right), \qquad (5)$$

with $\omega_d = -m\sqrt{gk}$.

A second-order scattering effect is due to the interactions between the electromagnetic wave and the others ocean waves. These interactions lead to a continuum level along the Doppler spectrum (also referred as the second-order continuum). This second order RCS is given by [4]

$$\sigma_2(\omega_d) = 8\pi k_r \sum_{m_1=\pm 1}\sum_{m_2=\pm 1}\int_0^{\infty}\int_{-\pi}^{\pi}\int_0^{\infty} S(m_1\vec{k}_1)S(m_2\vec{k}_2)\, \Gamma_p k^2 \sin c^2\left(\frac{\Delta r}{2}(k-2k_r)\right)\, \delta(\omega_d + m_1\sqrt{gk_1} + m_2\sqrt{gk_2})k_1 dk_1 d\theta_1 dk \quad (6)$$

with $\vec{k}_1 + \vec{k}_2 = \vec{k}_b$. g is the gravity and ΔR is the radial resolution. The coupling coefficient Γ_p is the sum of an electromagnetic coefficient and a hydrodynamic coefficient [17]. Thanks to this coefficient, the second order takes into account both the double scatterings and the second order hydrodynamic interactions.

For the sea directional spectrum $S(\vec{k})$, the non-directional Pierson-Moskowitz (function of the wind speed U_{10}) [6] and the standard form of the normalized directional distribution (function of the wind direction θ_w) [7] have been used. They are plotted in Fig.3. In Fig.3.a the dashed area delimits the major contribution of the sea spectrum in HF scattering.

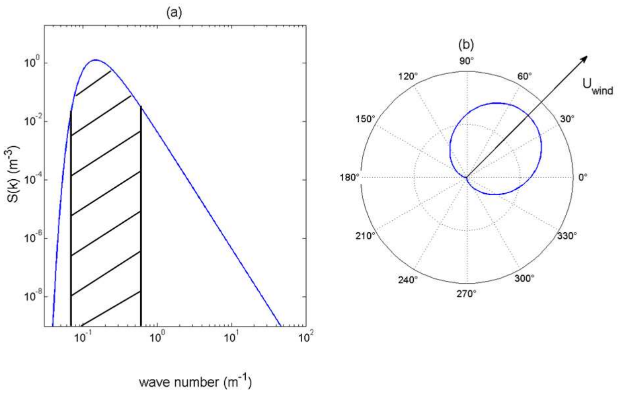

Figure 3. (a) non-directional spectrum of Pierson-Moskowitz for a wind speed U_{10}=6m/s. scattering. (b) normalized directional distribution for a wind direction θ_w=45°.

In Fig. 4 both the first and the second order for a radar frequency of 10MHz is plotted. The sea clutter is characterized by three pairs of peaks which are the most visible signature of sea clutter (Bragg peaks, second harmonic peaks, and corner peaks).

III. RANGE-DOPPLER IMAGE: ADDITION OF TARGET SIGNATURE, NOISE FLOOR AND PROCESSING EFFECTS.

A. *Background noise*

As it is suggested in [10], the background noise can be considered as an additive stationary Gaussian process. The corresponding spectral density P_N is given by [10]

$$P_N = k_b T_a 10^{F_{am}/10},$$

where k_b is the Bolzman constant and T_a is the ambient temperature. In HF, natural atmospheric, galactic radiation and man-made are mainly cause of background noise. According to its origin, background noise fluctuates significantly. In [13], one can find the following median value F_{am} = 36dB for f_r =10MHz.

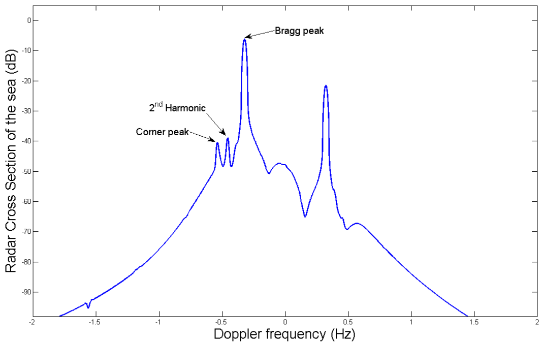

Figure 4. Doppler spectrum for a wind speed of 6m/s and for a difference between the radar direction and the wind direction of 45°.

B. *Target signature*

For our purpose it is not necessary to use a realistic model of the target scattering. We only consider the target as an additive (more or less punctual) scatterer with a given RCS σ_T. In the literature one can find for example that a small fast boat RCS is 10dB [8], a fishing boat RCS is 20dB [9], and a tanker RCS is 40dB [9]. So for a given range R_T and a given Doppler pulsation ω_T the following power is added in the Range-Doppler image

$$P_T = \frac{\lambda_r^2 P_t G_t G_r |F(R_T)|^4}{(4\pi)^3 R_T^4}\sigma_T \quad (7)$$

C. *Processing effects*

To enhance the model, we have considered how a Range-Doppler image is experimentally achieved from received power.

For radar transmitting a signal FMCW (Frequency modulated continuous wave) the radial resolution can be performed by range resolving FFTs [12]. The frequency resolution is achieved by a Fast Fourier Transform (FFT) of a sampled finite signal. These process considerations lead to decrease the range and frequency resolution and to add some secondary lobe. This is especially visible for the target signature. The main influent parameters are the integration time T_i for the frequency resolution and the bandwidth B and pulse duration of the transmitting signal for the frequency resolution.

D. *Range-Doppler image*

The simulated Range-Doppler image combines the sea, the background noise and the target powers, and includes the processing effects.

In Fig.5, the obtained Range-Doppler image is shown. For this simulation, the following parameters have been taken into account: U_{10}=5m/s, θ_w=20°, θ_r=90°, f_r=13MHz, B=100kHz, and T_i =60s. A target with a 30dB RCS has been added at range 90km and with a radial velocity of 15m/s.

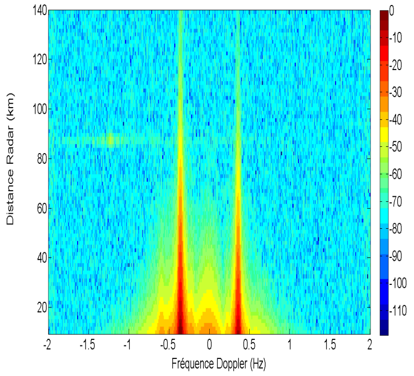

Figure 5. Simulated Range-Doppler image for U_{10}=5m/s, θ_w = 20°, θ_r = 90°, f_r=13MHz, B=100kHz, and T_i =60s. A target has been added with a RCS of 30dB, a range of 90km and a radial velocity of 15m/s.

To qualitatively evaluate the model, one can compare this simulated image with a Range-Doppler image obtained from real data (see Fig. 6).

There are expected differences. One can notice for example that in the model the sea state is considered homogeneous in the area of interest which is not the case with the real data. The effect is visible on the Bragg lines which are not perfectly strait in Fig. 6.

The fact that T_i is very short and the radar cross section of the sea is a random process can also explain differences (especially for the trails along Doppler dimension in real data).

In future works some enhancement will be considered. For example, the radar cross section of the sea will be considered as a random process.

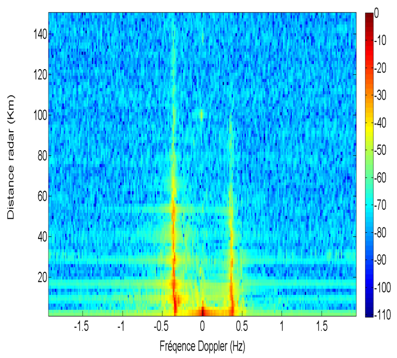

Figure 6. Range-Doppler image from real data.

IV. Target Detection

As already introduced, HFSW radars are potentially capable to detect and track targets at extremely long ranges. However, the performances of these systems are significantly limited by physical constraints, which are due to HF wave propagation and scattering, and interference presence (see Fig. 6). Moreover, the considered system is not optimized for target detection but for oceanographic remote sensing.

These last years, different approaches for target detection and tracking using HFSW radars have been proposed. They can use, for example, adaptive thresholding [14], CFAR-based methods [15] or a DWT-based method [16].

In this contribution, the idea is to extract the morphological components in the Range-Doppler image. The first one corresponds to directional elements which are due to the sea clutter (Bragg peaks, second harmonic peaks, and corner peaks) and interferences. To extract these components, a curvelet analysis is used. Then, an undecimated wavelet analysis is applied to extract the targets. This process, which is detailed in what follows, can be seen as a blind source separation technique.

Note that the theoretical backgrounds for the curvelet transform, the undecimated wavelet transform are not reviewed in this paper (because of limited space). The authors refer, for example, to [18, 19] for theoretical introductions.

A. *Target detection*

The first step is to extract/remove the sea clutter components in the image which are really damaging for the detection. In this way, a curvelet analysis is used. It allows to partially reconstruct the image after the curvelet decomposition (i.e. a percentage of the largest coefficients are selected and the others are cutoff). The obtained image contains essentially the directional components of the image. As an illustration, Fig. 7 shows the initial simulated Range-Doppler image and the obtained image after the partial curvelet reconstruction.

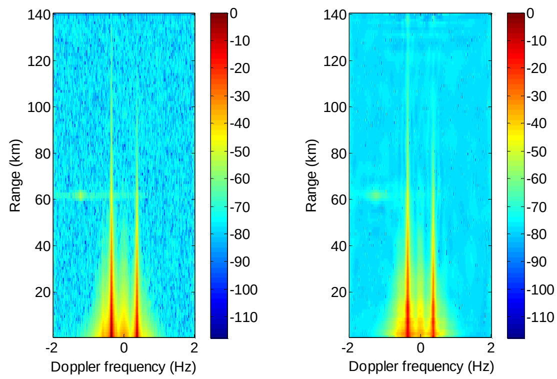

Figure 7. Simulated Range-Doppler image (left) and image containing (in its major part) the sea clutter components (right).

The next step (detection part) of the proposed approach is applied to the image resulting from the difference between the initial image and the one obtained after the curvelet-based treatment (see Fig. 8). An undecimated wavelet analysis with partial reconstruction is applied.

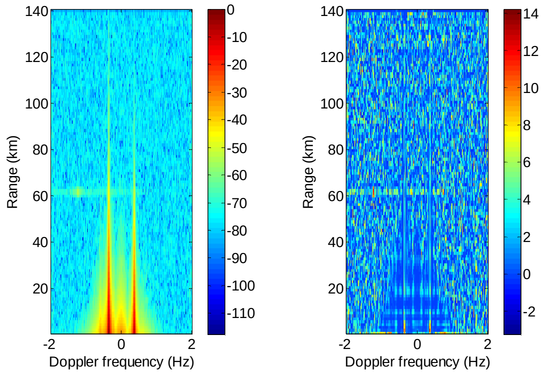

Figure 8. Simulated Range-Doppler image (left) and difference between the original image and the partially reconstructed image (right).

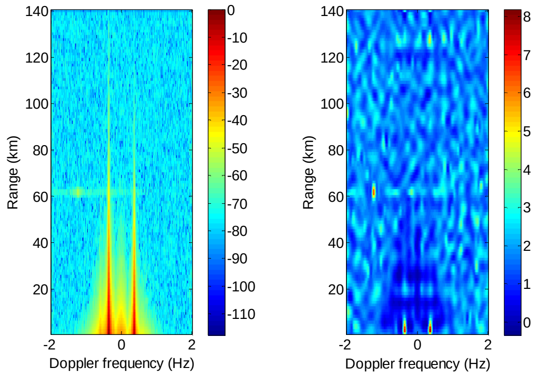

Figure 9. Simulated Range-Doppler image (left) and final image obtained after the curvelet and the UDWT analysis (right).

Figure 9 shows the obtained image. One can clearly see the target and some residual components at the bottom of the image. As it can be seen in the real Range-Doppler image, the measured data near the radar are really disturbed. Plus the first kilometers from the radar are not the object of this project so one can in practice eliminate the information in this area. Moreover within the first 30km microwave radars are more appropriate due to theirs better spatial and temporal resolutions.

In the proposed approach there are basically two parameters to be fixed which are the percentages of selected coefficients in the curvelet reconstruction and in the undecimated wavelet reconstruction.

B. *Detection capabilities against real data*

The real data are under consideration in this part. The goal is just evaluate and give a first idea of the detection capabilities of this approach.

Fig. 10, 11 and 12 show the original image in the left part of each figure and respectively the partially reconstructed image, the image resulting from the subtraction of the images in Fig. 10, and the final image (after UDWT partial reconstruction).

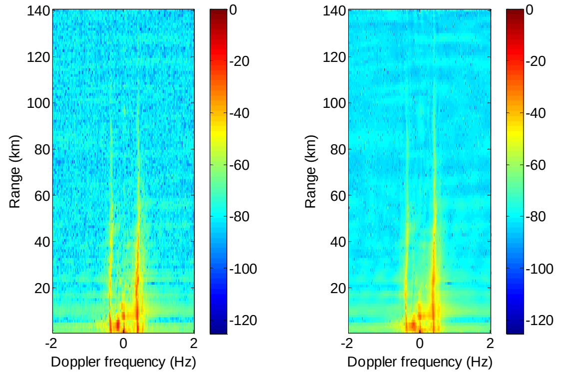

Figure 10. Range-Doppler image (left) and image obtained after partial curvelet reconstruction (right).

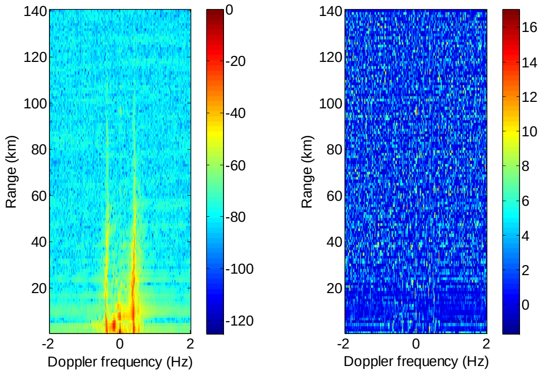

Figure 11. Range-Doppler image (left) and image resulting from the difference between the original image and the extracted sea-clutter-image (right).

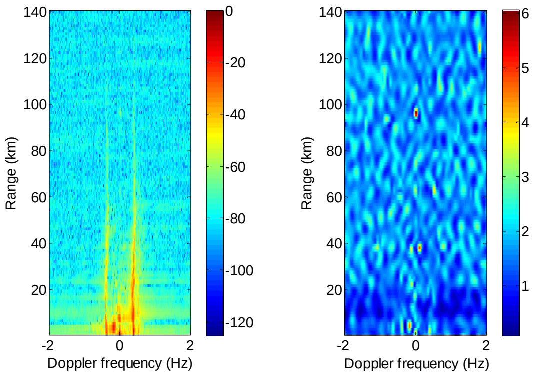

Figure 12. Range-Doppler image (left) and final image obtained after the UDWT analysis.

From these first results, one can notice the great potential of this approach. Of course, some complementary works have to be done. The authors remember that in this contribution their goal was to present a HFSW model for detection algorithm evaluation and to propose and show the capabilities of a new detection approach based on source extraction.

V. CONCLUSION

The main purpose of our project is to use HFSW radars, initially designed for remote sensing sea state, as a continuous maritime surveillance system. This means that the radar parameters are not optimal for target detection.

In this contribution, a Range-Doppler image model has been developed and qualitatively compared with real data. From this first comparison some enhancement will be (are already) considered in order to take into account more physical and processing effects phenomena.

Starting from this model a new target detection algorithm has been proposed. The obtained results on simulated data and the first results dealing with real data seem to be interesting. However, some complementary works must be done to precisely evaluate this approach and to increase the robustness and the estimation of the algorithm parameters.

ACKNOWLEDGMENT

The authors would like to thank the French institute SHOM and ACTIMAR for providing the real data.

REFERENCES

[1] A.N. Sommerfeld, “Propagation of Waves in Wireless Telegraphy, Annals Physic,” vol. 81, pp. 1135-1153, 1926.

[2] J.R Wait, “The Ancient and Modern History of EM Ground-Wave Propagation,” IEEE Antennas and Propagation Magazine, vol. 40, pp. 7-24, 1998.

[3] D.E, Barrick, “Theory of HF and VHF propagation across the rough sea 1 : the effective surface impedance for a slightly rough conducting medium at grazing incidence,” Radio Science, vol. 6, pp. 517-526, 1971.

[4] J. Walsh and E.W Gill, “An analysis of the scaterring of high-frequency electromagnetic radiation from rough surfaces with application to pulse radar operating in backscatter mode,” Radio Science, vol. 35, no. 6, pp. 1337-1359, 2000.

[5] D.E, Barrick, Remote sensing of sea state by radar, Oceans, 1972, vol. 4, pp. 186-192.

[6] W. Pierson, L. Moskowitz, “A proposed spectral form for fully developed seas based upon the similatity theory of S.A. Kitaigorodskii,” Journal Geophysic Research, vol. 69, no.24, pp. 5181-5190, 1964.

[7] M. Tucker, Waves in ocean engineering, New York : Ellis Horwood, 1991.

[8] T.M. Blake, The detctection and tracking of small fast boats using HF surface wave radar, BAE Systems, Marconi Reseach Centre, UK., 2000.

[9] M. Lesturgie, “Contribution de la technologie radar à onde de surface à la surveillance maritime depuis le littoral,” REE, Revue de l’électricité et l’électronique, no.3, pp 40-46, 2004.

[10] E.W Gill, J. Walsh, “A combined sea clutter and noise model appropriate to the operation of high-frequency pulsed Doppler radar in regions contrain by external noise,” Radio Science, vol. 43, RS4012, 2008.

[11] K.W. Gurgel, G. Antonischki, H.H. Essen, T. Schilck, “Wellen Radar (Wera) : a new ground-wave HF radar for ocean remote sensing,” Coastal Engineering, vol. 37, no. 3, pp. 219-234, August 1999.

[12] K.W. Gurgel, H.H. Essen, S.P. Kingsley, “HF radars : phycical limitation and recent developments,” Coastal engineering, vol. 37, pp. 201-218, 2000.

[13] International Telecomunication Union (1994) *Propagation in Ionized Media* (*ITU-R Recommendations, 1994 PI Series Volume*), ITU, Geneva, Switzerland.

[14] A.L. Dzvonkovskaya and H. Rohling, Adaptive Thresholding for HF Radar Ship Detection, Radiowave Oceanography - 6th International Workshop, May 2006, Hamburg, 2006.

[15] K.W. Gurgel and T. Schlick, HF Radar Wave Measurements in the Presence of Ship Echoes - Problems and Solutions, Oceans 2005 – Europe, vol. 2, 2005, pp. 937- 941.

[16] F. Jangal, S. Saillant, M. Hélier, “Wavelet Contribution to Remote Sensing of the Sea and Target Detection for a High-Frequency Surface Wave Radar,” IEEE Geoscience and Remote Sensing Letters, vol. 5, no. 3, pp. 552-556, 2008.

[17] W. Huang, E.W. Gill, J. Walsh, “Verification of the Second-Order HF Bistatic Radar Cross Section of ‘Patch Scatter’ on Ocean Surface,” IEEE NECEC, St. John's, Newfoundland, 2003.

[18] S. Mallat, “A wavelet tour of signal processing,” Academic Press, 1999.

[19] E.J. Candès, L. Demanet, D. Donoho, L. Ying, « Fast discrete curvelet transforms,” SIAM, Multiscale Modeling and Simulation, vol. 5, pp. 861-899, 2006.

[20] J.L. Starck, M. Elad, D.L. Donoho, “Redundant multiscale transforms and theirs application for morphological component separation,” Advances in Imaging and Electron. Physics, vol. 132, 2004.